Journal of Medicinal Chemistry

2-Aminopyridine-Based Mitogen-Activated Protein Kinase Kinase Kinase Kinase 4 (MAP4K4) Inhibitors: Assessment of Mechanism-Based Safety

Robert L. Dow, Mark Ammirati, Scott W. Bagley, Samit K. Bhattacharya, Leonard Buckbinder, Christian Cortes, Ayman F El-Kattan, Kristen Ford, Gary B. Freeman, Cristiano R. W. Guimaraes, Shenping Liu, Mark Niosi, Athanasia Skoura, and David Tess

Just Accepted

2-Aminopyridine-Based Mitogen-Activated Protein Kinase Kinase Kinase Kinase 4 (MAP4K4) Inhibitors: Assessment of Mechanism-Based Safety

Robert L. Dow,[*][†] Mark Ammirati,[‡] Scott W. Bagley,[‡] Samit K. Bhattacharya,[†] Leonard Buckbinder,[†] Christian Cortes,[†] Ayman F. El-Kattan,[†] Kristen Ford,[‡] Gary B. Freeman,[†] Cristiano R. W. Guimarães,[†] Shenping Liu,[‡] Mark Niosi,[‡] Athanasia Skoura,[†] David Tess[†]

[†]Pfizer Worldwide Research & Development, Cambridge, Massachusetts 02139, United States

[‡]Pfizer Worldwide Research & Development, Groton, Connecticut 06340, United States

ABSTRACT: Studies have linked the serine-threonine kinase MAP4K4 to the regulation of a number of biological processes/diseases including diabetes, cancer, inflammation and angiogenesis. With a majority of the members of our lead series (e.g. **1**) suffering from time-dependent inhibition of CYP3A4, we sought design avenues that would eliminate this risk. One such approach arose from the observation that carboxylic acid-based intermediates employed in our discovery efforts retained potent MAP4K4 inhibitory potency and were devoid of the TDI risk. The medicinal chemistry effort that led to the discovery of this CNS-impaired inhibitor together with its preclinical safety profile is described.

- INTRODUCTION

Mitogen-activated protein kinase kinase kinase kinase 4 (MAP4K4/HGK/ZCl) is a serine-threonine protein kinase[1] that has been shown to be involved in the regulation of a number of biological processes including inflammation,[2] cancer,[3,4] diabetes,[5] and angiogenesis.[6] MAP4K4 has been shown to regulate a number of cellular processes including cell transformation, adhesion,[3] and motility.[6,7] An impediment to understanding the signaling pathways involved in these biological effects is the lack of well characterized targets for MAP4K4. To date, NHE1,[8] Arp2,[9] ERM proteins[10] and FARP1[11] have been identified as phosphorylation substrates for this serine-threonine kinase. Selective inhibitors of MAP4K4 have served an important role in the initial steps of deconvoluting the signaling pathways of this kinase.[12-14]

Our group recently reported on a series of potent MAP4K4 inhibitors that arose from a virtual screening effort utilizing an in-house crystal structure of the kinase domain.[13] Optimized analogs contain a 2-aminopyridine core which establishes two points of contact with the hinge region of MAP4K4. As part of their binding to MAP4K4, these compounds also make a π-π interaction with

Tyr36, which is likely a driver in forming the unusual, folded P-loop structure of this kinase.[15] This feature is likely a contributor to the high level of kinome selectivity observed for this series of inhibitors.

In analogy to the *in vivo* response observed following treatment with a MAP4K4-siRNA,[16] inhibitor **1** reversed the inflammatory response induced by endotoxin (LPS) in a rodent model.[13] In a genetically-obese mouse model of insulin resistance, **1** performed comparably to the insulin sensitizer rosiglitazone in lowering blood glucose levels. While **1** possesses a number of positive attributes, analysis of its safety profile reveals several liabilities, including a positive response in the AMES genotoxicity assay and pharmacological promiscuity as demonstrated against a panel of non-kinase targets. Time-dependent inhibition (TDI) of CYP3A4 also led to drug accumulation following multi-day treatments with **1**, resulting in dose-limiting toxicities. Attempts to reduce the propensity for TDI through close-in structural modification approaches did not solve this problem.[13] Broader profiling of structural changes to the distal aminopyridine functionality, through incorporation of a range of neutral substituents to pyridyl/phenyl-based tail groups also failed to solve the TDI issue.[17] It is assumed that these modifications simply shifted the site of reactive species formation to the amine functionality of the aminopyridine core involved in hinge binding interactions with MAP4K4.

Replacement of the distal aminopyridine ring of **1** with an aminopyrimidine moiety (**2**) suppressed time-dependent inhibition of CYP3A4, eliminating both the genotoxicity and TDI-mediated drug accumulation risks. This modification also provided an improved off-target pharmacology profile.[13] Based on its *in vitro* safety and *in vivo* efficacy profiles, compound **2** was advanced to a rodent *in vivo* safety evaluation. Cardiovascular assessment was prioritized given the high association of this endpoint toxicity with the kinase inhibitor class.[18] Oral dosing in telemetered rats for five days with **2** (25 mg/kg, bid) resulted in a number of adverse effects. Substantial weight loss (7%) and body temperature increases (0.4^{o}C) relative to controls were observed over the course of the study. For cardiovascular endpoints, maximal heart rate increases of 25 bpm, relative to controls, were induced by treatment with **2**. Given that these effects were observed at free drug concentrations close to those required for inhibition of cellular kinase activity and *in vivo* inflammatory response,[13] further development of this compound was halted.

These safety findings also raised the question as to whether these toxicities were driven directly through inhibition of MAP4K4, the inherent chemotype or due to some off-target liability(s) that had not been identified in safety pharmacology profiling. To date, there have been no other reports of *in vivo* safety evaluation of a MAP4K4 inhibitor, making it difficult to place our own results in context regarding this question. Thus identification of an inhibitor which possessed an orthogonal off-target and/or exposure profile that could be advanced to an *in vivo* safety analysis provided the focus for the efforts disclosed here.

■   RESULTS AND DISCUSSION

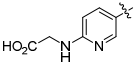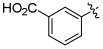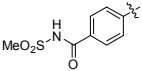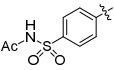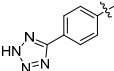With earlier efforts demonstrating that a wide range of structural modifications of either **1** or **2** led to compounds which retained significant liabilities, most notably TDI, alternative design approaches were required. Most of this subsequent work focused on

incorporation of polar functionality at various positions on the lead structure in an attempt to reduce CYP-mediated activation/TDI. An example of this was a set of amide analogs based on **3** (Table 1).[17] It was hoped that incorporation of a modestly polar/electron-withdrawing group in this terminal ring would impact the TDI potential. However, neither **3** nor a set analogs varying the nitrogen substituents of this lead provided a balanced potency/reduced TDI profile. In retrospect, the TDI associated with **3** is not too surprising given that it still retains significant turnover in human liver microsomes ($Cl_{int,app}$ = 22 uL/min/mg). Towards a goal of further reductions in oxidative metabolic liability, carboxylic acid intermediates **4** and **5** were evaluated. Both of these acids possessed potent MAP4K4 enzyme and modest cellular activity. The ability of this vector to tolerate an acid functionality is consistent with previous SAR on polar substituents in this position and our knowledge from MAP4K4 crystal structures.[13,15] More importantly, these acids were devoid of a TDI liability, as measured by the change in midazolam metabolism by CYP3A4, when treated with test compound in a dose responsive manner up to 60 μM. One potential explanation for the reduction in CYP inhibition by these compounds could be ascribed to the electron-withdrawing effect on the presumed reactive aminopyridine core by the carboxylic acid. The relatively low TDI associated with N-acetic acid analog **6**[19] suggests that this is likely not the key driver and the reduced TDI risk can be simply ascribed to low metabolic turnover for these carboxylic acids.[20]

Table 1. Enzyme, cell potencies, and time-dependent inhibition of CYP3A4 of analogs of compound **1**.
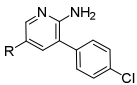
	R	Enzyme IC$_{50}$ (nM)[a]	Cell IC$_{50}$ (nM)[a]	TDI (%)[b]	Permeability[21] (x 10^{-6} cm/sec)
1		3.7	160	61	9
2		15	470	24	26
3		4.1	1182	59	12
4		21	3148	3	16
5		2.4	273	3	19

6		2.4	935	26	3
7		83	1121	--	--
8		7.6	1019	6	18
9		2.1	2018	--	5
10		5.6	1590	5	4
11		4.0	5388	57	7

[a]Geometric mean of ≥3 independent measurements run in triplicate [b]Change in midazolam metabolism by CYP3A4 after incubation with compound @ 60 uM @ 30 minutes.

In general, a right shift in cellular potency is observed for all members of this series, since they are ATP-competitive and the enzymatic assay is run at K_m ATP levels (10μM) vs cell-based concentrations which are in the millimolar range. This was confirmed through a similar right-shift in potency when the kinase assay was run in the presence of 1 mM ATP. Compound **5** inhibited MAP4K4 in a cell-based assay with an IC_{50} of 273 nM, which was in line with the potency in the enzyme assay run in the presence of 1 mM ATP (IC_{50} = 93 nM). This acid is highly permeable (P_{app} = 19 x 10^{-6} cm/sec)[22] and demonstrated no evidence of efflux based on PgP ratios, suggesting these properties are not drivers in the right-shifted cellular potency.

In order to make certain that incorporation of a carboxylic acid did not adversely affect the off-target profile of this series, **5** was screened against kinome and pharmacology panels. Screening against twenty kinases at 10 μM revealed that **5** inhibited only two non-MAP4K4 family kinases, Aurora and ABL, to a substantial extent (Supporting Information).[23] Follow-up screening in cell-based systems containing these two kinases revealed that **5** had an IC_{50} > 30 μM against each. A clean profile (IC_{50} > 10μM) was also observed against a panel of ~20 common secondary pharmacologic targets (Supporting Information). In summary, the finding that carboxylic acid substituents are compatible with potent, selective MAP4K4 inhibition provided a forward path for this chemotype, ultimately leading to the identification of an orthogonal profile which could be advanced to a safety evaluation.

Given that the carboxylic acid had been incorporated at a site on the core structure that was expected to be near the solvent/protein interface when bound to MAP4K4, it raised the question of whether this group was interacting with the protein and contributing to the observed potency. To gain insight into this question unsubstituted congener **7** was prepared. Removal of the acid led to ~30-fold reduction in enzyme potency, suggesting the acid functionality has a direct interaction with MAP4K4. Since

attempts to generate a crystal structure of **5** bound to MAP4K4 were not successful it is not clear what interaction(s) might be occurring between the acid and protein. Moving the carboxylic acid into the 3-position (**8**) led to only a slight reduction in potency.

A limited set of carboxylic acid bioisosteres were explored (**9-11**) and found to be potent inhibitors of the MAP4K4 kinase domain. A significant right-shift in cellular activity was observed for all of them relative to the **5**. This may in part have been driven by the reduced passive permeability of these isosteric analogs compared to **5** (Papp = 2, 6 and 4 x 10^{-6} cm/s for **9-11**, respectively). Further efforts on bioisosteric replacements were not pursued based on this profile, as well as their relatively high polar surface areas (93-110 Å^2), since these properties would limit optimization efforts with regards to incorporation of additional polar substituents (e.g. modification of the chlorophenyl ring). Interestingly, tetrazole **11** also carries significant TDI risk even though it has low turnover in human microsomes (Cl$_{int,app}$ < 8 uL/min/mg).

Utilizing library-enabled chemistry the structure-activity-relationships for the p-chlorophenyl substituent were developed. Representative examples selected from the ~120 analogs prepared are shown in Table 2. The *in vitro* profiles of the des-chloro (**12**) and m-chloro (**13**) analogs were slightly right-shifted relative to **5**. Ortho substitution on this ring with substituents possessing a range of electronic/steric properties was not well tolerated (e.g. **14**). This is consistent with MAP4K4 crystal structures bound to this class of inhibitors which reveal an extended tunnel-like region in the protein that surrounds the phenyl group with tight tolerances for the ortho vectors.[13] Consistent with these earlier SAR/structural studies, the 4-position of this series tolerated a wide range of substituents (e.g. **15-19**). MAP4K4 residues lining this pocket are hydrophobic in nature, suggesting that heteroaromatic replacements for the chlorophenyl substituent would not be well tolerated. This was borne out by the finding that pyrimidine **20** was >50-fold less active relative to **19**. From a small set of heteroaromatic replacements, N-methylpyrazole **21** was identified as a potent inhibitor of the catalytic domain of MAP4K4, but was inactive in the cell assay. Given concerns around the physical properties associated with the triaryl series, replacements for the chlorophenyl ring were explored. Incorporation of a phenoxymethyl group in the 3-position of the aminopyridine (**22**) led to ~10-fold reduction in enzyme/cellular MAP4K4 inhibitory potency. Incorporation of the regioisomeric ether linker (**23**) led to increased inhibitory potency relative to **22**. Cyclobutylmethyl ether **24** had comparable potency relative to the corresponding benzyl ether. This isosteric replacement of an aryl with a cyclobutyl ring is consistent with the binding pocket in this region being formed by aliphatic-based amino acid residues in MAP4K4.

Of the analogs in Table 2 tested for time-dependent inhibition of CYP3A4, only ether **23** demonstrated significant activity at 60 µM (41%). The highly electron-rich nature of this particular aminopyridine is likely the driving force behind the formation of reactive intermediates. While ethers **23** and **24** demonstrated good *in vitro* inhibitory profiles, further efforts around these alkoxymethylpyridine cores were not pursued given their associated TDI risk.

Table 2. Enzyme and cell potencies of aryl analogs of **4**.

	R	Enzyme IC$_{50}$	Cell IC$_{50}$	Permeability[21]
		(nM)^a	(nM)^a	(x 10^{-6} cm/sec)
12		12	1692	17
13		11	1308	16
14		62	>10000	--
15		7.6	1019	17
16		3.5	248	13
17		7.2	3391	12
18		6.0	491	15
19		3.5	377	13
20		238	>10,000	--
21		13	>10,000	5
22		43	>8500	13
23		11	4006	17
24		11	1852	18

^{a} Geometric mean of ≥3 independent measurements run in triplicate.

With these early studies suggesting that the benzoic acid moiety played a significant role in both MAP4K4 inhibitory activity and suppression of TDI, our attention turned to development of the carboxylic acid SAR. Having failed to successfully obtain co-crystals of **5** or related analogs with the catalytic domain of MAP4K4, an empirical approach was employed. Homologation to

acetic acid **25** maintained MAP4K4 enzymatic and cellular potency (Table 3). While this compound had low projected human clearance based on human liver microsomes ($CL_{int,app,scaled} < 8$ mL/min/kg), analysis in rat liver hepatocytes suggested moderate to high clearance ($CL_{int,app} = 62$ uL/min/million). Intravenous dosing in rats confirmed this prediction (CL = 8 mL/min/kg, 1 mg/kg) and suggested that further *in vivo* analyses in efficacy/safety models might be hampered by this profile, especially given the low free drug fraction in this species (fu = 0.004). Regioisomeric analog **26** also potently inhibits MAP4K4, however, kinome profiling suggested that it had reduced selectivity relative to the **25** (Supplementary Information). Incorporating the dimethyl substituents of **25** into carbo-/heterocycles (**27-29**) retained potent inhibitory activity. Unlike in the case of the benzoic acid leads, conversion of the carboxylic acid in **27** to the corresponding tetrazole (**29**) did not lead to a significant reduction in cellular potency. Besides a low predicted permeability ($P_{app} = 1 \times 10^{-6}$ cm/sec), **29** was also found to potently inhibit phosphodiesterase 5A1 ($IC_{50} = 27$ nM). Tying the benzylic position of the acetic acid pharmacophore back as part of a indane ring (**30/31**) also resulted in potent inhibition, with **30** being 10-fold more potent than its enantiomer. While **30** had an improved profile vs PDE 5A1 activity ($IC_{50} = 3.4$ uM), it had moderate turnover in both human and rat hepatocytes ($CL_{int,app} = 12$ and 67 uL/min/million, respectively).

In contrast to earlier carboxylic acid-based analogs, a 2.5Å structure of **27** bound to the catalytic domain of MAP4K4 was successfully generated (Figure 1). In analogy to other crystal structures for this series, the aminopyridine makes acceptor-donor interactions with the hinge region of the enzyme.[13] The structure also reveals that the acid is interacting with the backbone N-H of Gly32, which is at the start of the P-loop structure.[15] This interaction assists in stabilizing this protein feature that forms the hydrophobic tunnel accommodating this series of inhibitors. The carboxylic acid is sitting at the interface of the opening of this pocket and solvent-exposed space (Figure 2). Replacement of the carboxylic acid with a nitrile (**32**) results in a 300-fold reduction in MAP4K4 inhibitory potency, which is consistent with the nitrile being unable to make a productive interaction with the P-loop region of the enzyme.
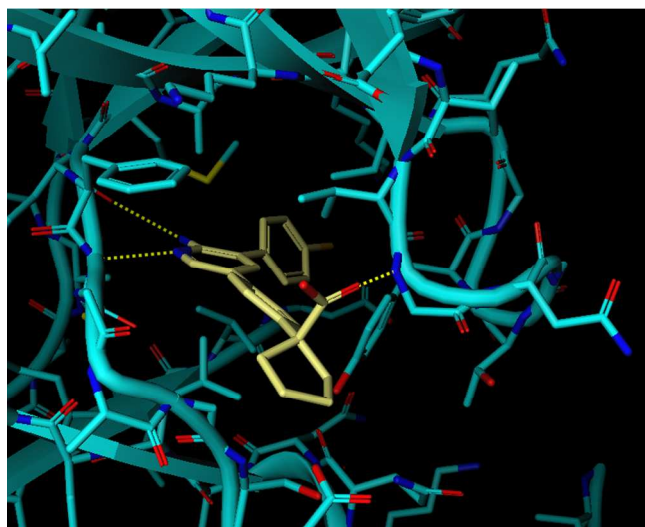
Figure 1. Crystal structure (2.5 Å resolution) of the complex between the catalytic domain of MAP4K4 and compound **27** (in yellow) (PDB code: 5J95).

Based on the interactions identified from the crystal structure of **27** bound to MAP4K4, lengthening of the linker between the phenyl ring and the carboxylic acid did not appear at first to be a fruitful avenue for pursuit. To assess the validity of this conclusion, propionic acid derivative **33** was prepared and screened for MAP4K4 inhibitory activity. This homologated acid retains substantial enzymatic and cellular potency, suggesting the carboxyl acid in this case may be picking up productive interactions with the protein further outside of the hydrophobic tunnel than Gly-25.

Replacement of the propionic acid sidechain with the isosteric oxyacetic acid (**34**) led to a 4-fold improvement in MAP4K4 enzyme inhibitory activity, but a 10-fold reduction in cellular activity relative to **33**. This substantial shift in cellular activity is likely not explained by differences in passive permeability (P_{app} = 7 and 12 x 10^{-6} cm/sec, respectively). To further address this question, a series of analogs were prepared in which additional lipophilicity was introduced in the α-position. Methyl enantiomers **35** and **36** retain potent inhibitory activity, with **35** showing a modest improvement in cellular potency compared to **34**. Incorporation of a dimethyloxyacetic acid tail (**37**) led to sub-nanomolar enzymatic potency, as well as a further improvement in cell activity. This modification also favorably impacted turnover in human and rat hepatocytes $CL_{int,app}$ < 6 and < 25 uL/min/million, respectively) in addition to further separation from the off-target PDE5A1 activity (IC_{50} = 1.9 uM). To determine whether the carboxylic acid in **37** was a key driver of MAP4K4 potency, isopropyl ether **38** was prepared. In line with the earlier work around the benzoic acid analogs, removal of the carboxylate group led to ~3,000-fold loss in enzymatic potency and ~25-fold right-shift in cellular potency. The moderate permeability of **37** (P_{app} = 10 x 10^{-6} cm/sec) may be a contributing factor in the differential shift in cellular potency relative to enzymatic potency for **38**. An attempt to increase cell permeability through incorporation of a cyclopentyl ring (**39**) actually had the opposite effect (P_{app} = 3 x 10^{-6} cm/sec) and in fact resulted in an isolated enzyme to whole cell ratio consistent with that seen for **37**. These results further underscore the conclusion that multiple drivers are in play for this translation between these *in vitro* activities. Additional close-in structural modifications of **37**, such as *m*-isomer **40** or incorporation of a pyridine ring (**41**), in analogy to **1**, did not provide an improved profile. Finally, extension of the linker length between the phenoxy ring and carboxylic acid (**42**) resulted in modest enzymatic/cellular potency.
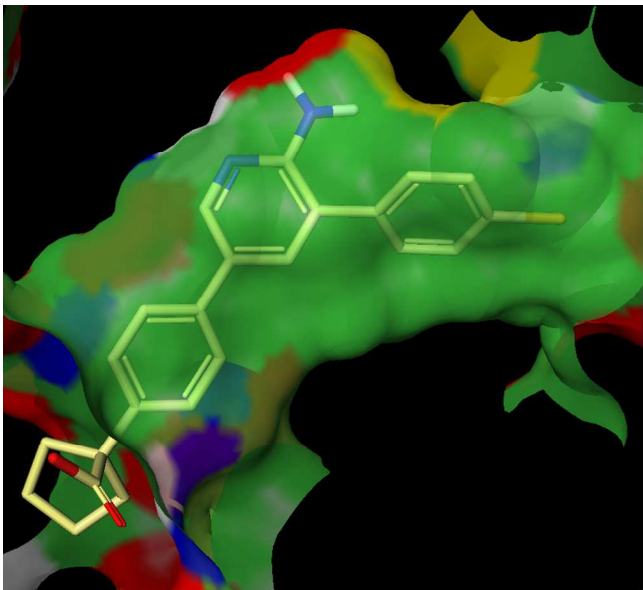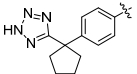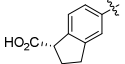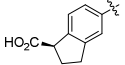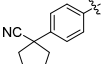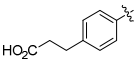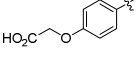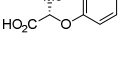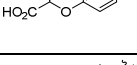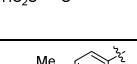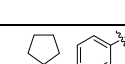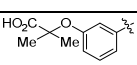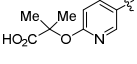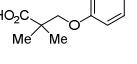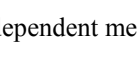
Figure 2. Rendering of protein surface area of the catalytic domain of MAP4K4 bound to compound **27** (in yellow) (PDB code: 5J95).

Attempts to co-crystallize **37** with the catalytic domain of MAP4K4 were not successful. Modeling of this ligand into the crystal structure obtained with **27** suggests that it is unlikely the acid of **37** is interacting with the backbone N-H of Gly32.

Table 3. Enzyme and cell potencies of benzoic acid modifications of **5**.
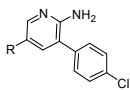
	R	Enzyme IC$_{50}$ (nM)[a]	Cell IC$_{50}$ (nM)[a]	Permeability[21] (x 10^{-6} cm/sec)
25		3.5	231	11
26		1.4	407	10
27		4.6	148	3
28		2	101	10

29		2.9	331	1
30[b]		1.4	103	13
31[b]		15	1052	12
32		1426	--	--
33		8.1	602	--
34		2.0	5574	7
35[b]		1.0	842	5
36[b]		7.9	8728	5
37		0.4	222	8
38		1421	4699	--
39		0.6	467	3
40		2.0	564	10
41		1.3	197	9
42		6.5	470	4

[a] Geometric mean of ≥3 independent measurements run in triplicate. [b] Absolute stereochemistry arbitrarily assigned.

Based on its overall profile, oxyacetic acid analog **37** was selected for further evaluation. A summary of key *in vitro*/ADME/safety properties of this acid relative to the aminopyridine-based starting point **1** is detailed in Table 4. Incorporation of the carboxylic acid resulted in an improved turnover in human microsomal/hepatocytes, with no detectable metabolism observed for **37** in either of these systems. As for the other carboxylic acid-based analogs in this series, the risk of TDI was also eliminated, which in turn is likely responsible for the differential mutagenic risk between these two compounds, as evidenced by the AMES results. Screening (10 µM) against a panel of 58 off-target pharmacologies showed a

very clean profile, with only 5-hydroxytryptamine receptor 1B and ACE showing >50% effect. Both of these targets were

evaluated in functional assays and **37** showed no significant activity for either at concentrations up to 30 μM (Supporting

Information). Based on the selective kinome profile of related members of this series, **37** was screened in human peripheral

blood cell lysates for inhibitory activity against a panel of 232 kinases (ActivX screen). Other than MAP4K4/MINK/TNIK,

only STE kinome branch member germinal center kinase (GCK/MAP4K2) and the lipid kinase phosphatidylinositol-5-

phosphate 4-kinase, type II, gamma (PIP4K2C) were inhibited >70% by **37** (1 μM). Comparable potencies for the close-in

family members MINK and TNIK were confirmed by enzymatic screening at Km levels of ATP, with IC_{50} = 1.3 and <0.6

nM, respectively. Profiling against a set of 244 kinases screened in the presence of 1 mM ATP and 1 μM **37** revealed less

than 50% inhibition by all these targets (Supporting Information). With an IC_{50} of 6 nM against MAP4K4 under physiologi-

cal ATP concentrations, these results suggest that compound **37** possesses a high degree of kinome selectivity.

Table 4. MAP4K4/Physicochemical/ADME profiles for **37/1**

Properties	37	1
MAP4K4 kinase domain IC_{50} (nM) @ [ATP] = 10 μM[a]	0.4	3.7
MAP4K4 kinase domain IC_{50} (nM) @ [ATP] = 1 mM[a]	6	134
Cell IC_{50} (nM)[a]	222	160
MW/eLogD/TPSA[b]	383/1.2/85	296/3.3/78
HLM $Cl_{app,scaled}$ (mL/min/kg)	<8	42
hHepatocyte $Cl_{int,app}$ (μL/min/million)	<4	31
Solubility, pH 1.2, mg/mL	1.4[c]	13[d]
pH 6.5, mg/mL	0.14[c]	5.8[d]
Permeability (x 10^{-6} cm/sec)	10	3
CYP inhibition IC_{50}[e]	>3 μM	>3 μM
TDI, %Inhibition (Dose)[f]	-4% (30μM)	54%

	(30μM)	
	3% (60μM)	61%
	(60μM)	
hERG IC_{50}[g]	~100 μM	1.8 μM
THLE IC_{50}[h]	>250 μM	>119 μM
AMES[i]	Negative	Positive

[a]Geometric mean of ≥3 independent measurements run in triplicate; [b]eLogD = measured logD at pH 7.4; [c]monohydrate solvate [d]di-hydrochloride salt; [e]<15% Inhibition at 3uM for isoforms (3A4, 2D6, 1A2, 2C8 and 2C9) [f]Change in midazolam metabolism after incubation with compound @ 30 minutes[23] [g]Measurement of potassium current in human embryonic kidney 293 (HEK293) cells stably transfected with the human ether-a-go-go-related gene (hERG) channel [h]Transformed human liver epithelial cell assay, (THLE)[24] [i]Activity in a bacterial mutagenesis assay.[25]

Compound **37** was advanced to pharmacokinetic profiling in anticipation of efficacy/safety studies. Consistent with their respective microsomal turnover values, intravenous dosing in rat, dog and non-human primate confirmed low clearance. Moderate to long half-lives were observed in all species, along with low volumes of distribution (Table 5). Predicted human clearance based on either human microsomal/hepatocyte data or allometric scaling suggested low human clearance.

Table 5. Pharmacokinetic profile of **37**.

	Rat[a,b]	Dog[a,c]	NHP[a,d]
Clearance (mL/min/kg)	0.76	1.5	0.90
$T_{1/2}$ (hr)	3.7	2.0	10
Volume (L/kg)	0.25	0.42	0.52

[a]Dosed at 1 mg/kg, i.v.; [b]Fed male Wistar Han (n=2); [c]Fed male beagle (n=2); [d]Fasted male cynomolgus (n=2).

In preparation for *in vivo* safety evaluation of **37** a PK/PD analysis was carried out in the same model system utilized to evaluate MAP4K4-siRNA inflammatory efficacy.[2] Mice were dosed orally with inhibitor followed by an injection of lipopolysaccharides (LPS) after 30 minutes. Plasma changes in TNFα were measured at 1.5 h and the corresponding free drug levels determined (Fig-

ure 3). While TNFα levels were elevated at the lower drug doses in multiple experiments, it was assumed that it was not a drug-related effect given that the free concentrations at these doses were below the cellular IC_{50}. Only the top two dose groups exhibited substantial suppression of TNFα release upon stimulation with LPS, which is consistent with their corresponding free exposures being greater than the MAP4K4 cellular potency of **37**.
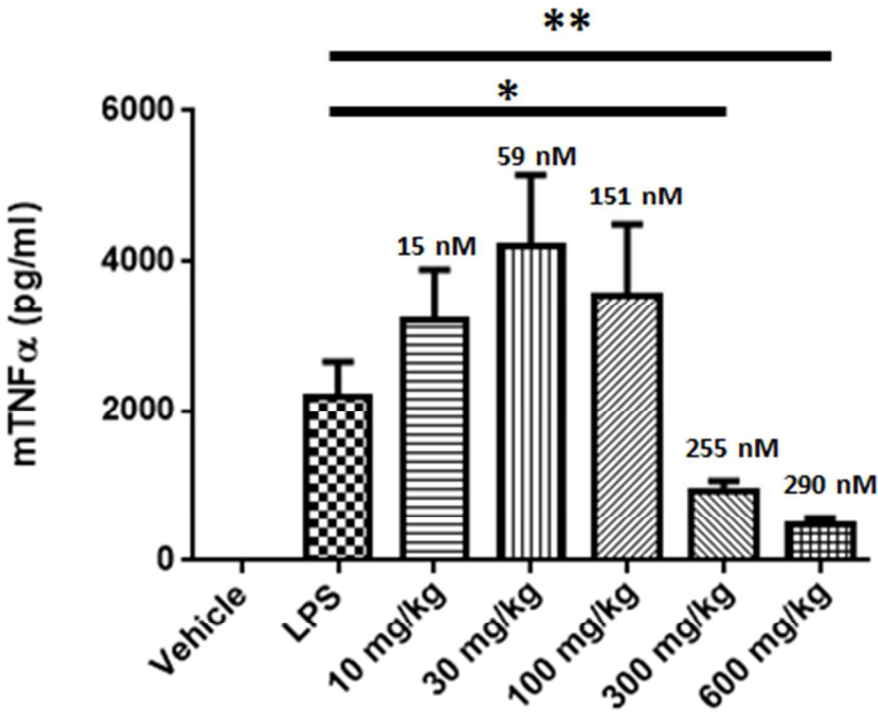
Figure 3. Dose-response effects of **37** on LPS-induced TNFα levels in male C57-BL/6J mice (p.o., 0.5% methylcellulose vehicle). *p=0.0002, **p=0.0001. Average free concentrations of **37** are shown above each dose bar in the graph.

   In considering additional MAP4K4 chemotypes to advance to safety studies, carboxylic acids afforded the potential to design in a peripherally-restricted exposure profile. Exclusion from the brain would aid our understanding of whether safety signals, such as the reduced food intake and body temperature, observed for **2** were centrally-mediated.[26] To assess whether **37** had the potential to be excluded from the brain it was screened for efflux potential in MDCK-MDR1(NIH)[27] and BCRP[28] containing cell lines. In both of these assay systems **37** exhibited a profile suggesting high efflux potential, with MDR1- and BCRP-based BA/AB ratios of 3 and 116, respectively. These results were shown to be predictive, with an average free drug brain/plasma ratio of 0.14 over a 5-hr test period after an oral dose of 10 mg/kg of **37** in rats. The overall profile of this brain-impaired inhibitor led us to advance it to general toxicology and cardiovascular safety profiling.

   No significant changes in clinical signs were observed following a single oral dose of 500 mg/kg of **37** in rats. The average free drug concentration over this 24 hr period was 143 nM. Achieving high free exposure levels in rodent species was particularly chal-

lenging given the extremely high protein binding (rat fu_{plasma} = 0.0005). In this single dose rat study the $C_{max,free}$ was just 250 nM. The relatively low peak concentrations for this compound help to minimize the chance of off-target effects skewing interpretation of these safety evaluations. Based on its clean profile in this single-dose study, **37** was advanced to a dose escalation study in dogs. Exposure was limited in this study due to emesis occurring at all doses, with $C_{avg,free}$ = 50, 85 and 293 nM at 20, 100, 500 mg/kg, respectively. The only clinical sign observed in any of the treatment groups was mucoid feces and transient tremors in one of the two dogs receiving 500 mg/kg. To determine whether **37** was differentiated relative to the negative cardiovascular effects observed for **2**, a sling-trained dog cardiovascular evaluation was performed. No significant changes were observed during a stepwise esca-lating *i.v.* infusion of **37** for either blood pressure or heart rate at free drug concentrations up to 40-fold the C_{eff} determined in the LPS assay. Based on this encouraging set of single-dose data, **37** was advanced to a 2-week rat safety study (20, 100 and 500 mg/kg/day, p.o., b.i.d. dosing). Average $C_{avg,free}$ exposures at these doses on the first day of dosing were 15, 67 and 166 nM. Con-sistent with **37** showing no significant activity in the *in vitro* TDI assay, inter-animal day 1and 14 exposures did not vary substan-tially. While no effect on body weight or food intake were observed at the two lower doses, at the highest dose there was a reduc-tion of body weight gain (0.66x) and food intake (0.8x) relative to control animals. By day 4, animals in the high dose group start-ed to exhibit a number of signs of moribundity and there was a death of one animal, leading to termination of the study. The effects observed in this group mimicked very closely what was observed in a five-day evaluation carried out in rats with **2**. As in this pre-vious case, profound toxicity was observed at exposures close to efficacious concentrations.

The significant toxicology signals associated with **2** and **37** are suggestive of a MAP4K4-driven safety liability. This is supported by their high MAP4K4-specificity, differential exposure profiles and the relatively low concentrations leading to these safety find-ings. It is important to note that these inhibitors also inhibit the other kinase family members, MINK and TNIK, which could also be contributing to the observed effects. Addressing this issue will likely require development of an allosteric MAP4K4 inhibitor. Such a compound would have the benefit of high kinome specificity, including MAP4K4-family selectivity, and the potential to achieve efficacy at much lower concentrations given its non-ATP competitive nature.

- ▪ SYNTHESIS

Synthesis of the inhibitors described and characterized herein relied mainly upon a Suzuki-Miyaura cross coupling reaction to form the bond between the aminopyridine core and the acidic tail aromatic ring.[29] Representative synthetic approaches utilized in this study can be found in Schemes 1-3. Reaction of aminopyridine-based boronate **43**[13] with bromoester **44** under standard Suzuki-Miyaura coupling conditions provided ester **45**. Cleavage of the *t*-butyl ester with acid afforded acid **3**.

Scheme 1^a
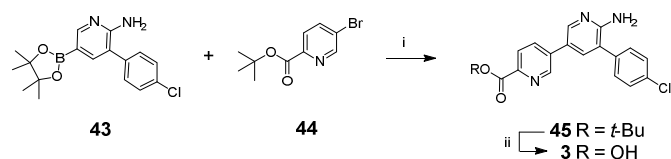
^aReagents and conditions: (*i*) Pd(dppf)Cl$_2$, Na$_2$CO$_3$, 1,4-dioxane, H$_2$O, 85 °C; (*ii*) HCl, EtOH, CH$_2$Cl$_2$, RT.

_____

An alternative approach to the preparation of compounds possessing variations of the acid-containing aromatic tails is to reverse the reactivity of the two partners in the Suzuki-Miyaura reaction. Scheme 2 details this approach utilized for the synthesis of **37**. Bromide **46** was converted to the corresponding boronate ester **47**. Coupling of this boronate with bromoaminopyridine **48** under Suzuki-Miyaura conditions provided ester **49**. Base hydrolysis afforded the target oxyacetic acid-based derivative **37**.

_____

Scheme 2^a
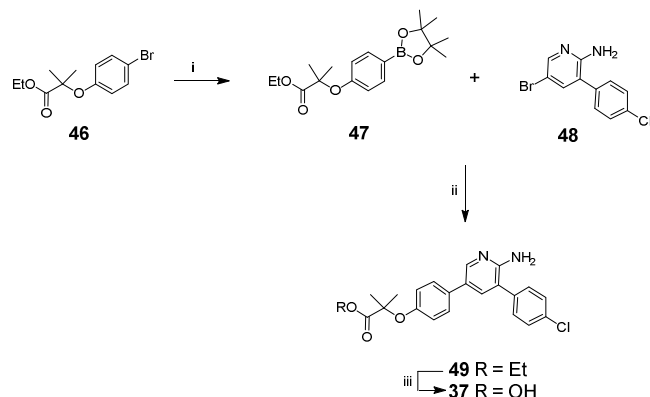
^aReagents and conditions: (*i*) 4,4,4',4',5,5,5',5'-octamethyl-2,2'-bi-(1,3,2-dioxaborolane), Pd(dppf)Cl$_2$, KOAc, 1,4-dioxane, 80 °C; (*ii*) Pd(AmPhos)$_2$Cl$_2$, Na$_2$CO$_3$, EtOH, H$_2$O, 60 °C; (*iii*) NaOH, H$_2$0, EtOH, reflux.

_____

An approach for rapid development of structure-activity-relationships in the 3-position of the aminopyridine head group was developed in which a late stage 3-bromo intermediate was utilized (Scheme 3). This intermediate was generated via a two-step sequence involving a Suzuki-Miyaura coupling of boronic acid **50** and aminobromopyridine **51** to afford biaryl **52**. Subsequent bromination of the intermediate with N-bromosuccinimide provided **53** in 81% overall yield for this sequence. Coupling of this bromide with phenyboronic acid afforded ester **54**. Acid catalyzed cleavage of the *t*-butyl ester afforded acid **12** as the TFA salt.

_____

Scheme 3[a]
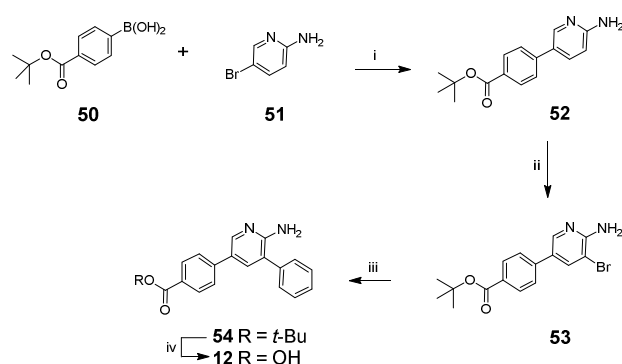
[a]Reagents and conditions: (*i*) Pd(dppf)Cl$_2$, Na$_2$CO$_3$, 1,4-dioxane, H$_2$0, 80 ^{o}C; (*ii*) N-bromosuccinimide, CH$_2$Cl$_2$, RT; (*iii*) phenyl-boronic, Pd(dppf)Cl$_2$ acid, K$_2$CO$_3$, 1,4-dioxane, H$_2$0, 80 ^{o}C; (*iv*) trifluoroacetic acid, CH$_2$Cl$_2$, 30 ^{o}C.

_____

CONCLUSION

Incorporation of an oxyacetic acid moiety into a lead series of MAP4K4 inhibitors afforded high target potency and selectivity. This modification also provided a significant degree of CNS-impairment, which was viewed as a positive attribute for targeting disease endpoints such as diabetes and other inflammation-driven indications. While this profile was distinct when compared to early members of this series, a similar preclinical safety profile was still observed. These results are suggestive that inhibition of MAP4K4 and/or its closely-related family members being responsible for eliciting these safety signals. Alternative approaches, such as the identification of non-ATP competitive inhibitors, would be of value in assessing this hypothesis.

EXPERIMENTAL SECTION

All procedures performed on these animals were in accordance with regulations and established guidelines and were re-

viewed and approved by Pfizer Institutional Animal Care and Use Committee.

MAP4K4 Z'-Lyte Assay. The *in vitro* kinase assay utilized human recombinant protein, GST-tagged MAP4K4 catalytic

domain, residues 1-328 (Invitrogen #PV4013) and the Z'-Lyte Ser/Thr 7 FRET peptide substrate (Invitrogen #PV3208)

which is labeled with fluorescein and coumarin. This FRET assay is based on the differential sensitivity of phosphorylated

and non-phosphorylated peptides to proteolytic cleavage using methods outlined by the manufacturer (Invitrogen). The assay

was optimized for a MAP4K4 concentration that phosphorylated 20-40% of the Z'-Lyte Ser/Thr 7 peptide at Km ATP (10

µM, Invitrogen #PV3227) in a 90 min reaction at room temperature (RT; 1.25 nM). The 10 µL reactions were carried out in

384-well black Optiplate (Perkin Elmer #6007279) in assay buffer (50 mM HEPES pH 7.5, 1 mM EGTA, 10 mM $MgCl_2$,

and 0.01% Brij-35; Invitrogen #PV3189), containing 0.5% compound/DMSO, 2 µM Z'-Lyte Ser/Thr peptide, 1.25 nM

MAP4K4, and either 10 µM ATP (Km) or 1 mM ATP ("physiological levels"). The phosphorylation range was determined

using 0% and 100% phosphorylation controls. ATP is omitted in 0% phosphorylation controls. The 100% phosphorylation

controls used a phosphorylated standard of the Ser/Thr peptide (2 µM; Invitrogen # PV3223) in place of enzyme, peptide and

ATP. Enzyme and compound were incubated for 30 min at RT before ATP addition. Reactions were carried out for 25 min

in the presence of 1 mM ATP, or for 90 min in the presence of 10 µM (Km) ATP at RT (optimized to achieve 20%-40%

phosphorylation). At 60 min, 5 µL of Development Reagent A diluted in Development Buffer was added to each well

(1:65,536; Invitrogen #PV3295, PV3127) and incubated for 60 min at RT. The reaction is stopped with 5 µL Stop Buffer

(Invitrogen #PV3094), shaken for 30 sec and read immediately on a Perkin-Elmer Envision in FRET mode (excitation filter,

Photometric 405 (barcode 302), emission filter 1, FITC 535 (barcode 206), emission filter 2, Umbelliferone 460 (barcode

207)). Percent inhibition was calculated based on sample wells containing either DMSO only (0% inhibition) or a standard

compound (100% inhibition). Compound concentration-responses were fit to a 4-parameter equation to determine compound

IC_{50} values.

MAP4K4-traf2 Cell ELISA.

The assay was designed to identify compounds inhibiting MAP4K4's phosphorylation of serine/threonine residues on traf2.

GripTite™ 293 MSR Cells (Life Technologies #R795-07) were maintained in complete media (DMEM #11965-092 with

10% FBS, 10 mM HEPES (#15630-080), 1x MEM NEAA (#11140-050), 600 µg/mL Geneticin (#10131-027) and 1,000

U/mL Penicillin/Streptomycin (#15140-122, Life Technologies). For culturing and plating, cells were washed with cation-

free DPBS (Lonza #17-512Q) and incubated 5 min at room temperature (RT) with 37°C Versene (Life Technologies

#15040-066). After decanting, 5 mL 0.25% Trypsin-EDTA (Life Technologies #25200-056) was added and the flask gently

rocked to loosen cells. Cells were passaged 1:15 in complete media. An in-well transient transfection was performed. Cells

were seeded at 35,000 cells/well in 100 μL complete media in 96-well polystyrene TC-coated plates (Corning #3598). After

15 min at RT, plates were moved to a 37 °C, 5% CO_2, humidified incubator for 6 h. To transfect one plate of cells, 25 μL

FuGENE® HD (Promega #E2311) was added to 500 μL OptiMEM prewarmed to 37 °C (Life Technologies #31985-070)

and incubated for 5 min at RT. 8.75 μg of pcDNA3.1-traf2-FLAG tag (*NM_001242559.1*) and 3.5 μg of pcDNA3.1-

MAP4K4-myc-His tag (*NM_021138.3*) were added to the OptiMem mixture, gently mixed and incubated for 15 min at RT.

The DNA-Fugene mix was diluted with 2.625 mL OptiMem, and 25 μL was dispensed to each well of plated cells. The

plates were gently swirled before moving back to the 37 °C, 5% CO_2, humidified incubator for 40 h. The cells are treated

with compound solubilized in DMSO, diluted in complete media, for a final DMSO concentration of 0.25%. The plates were

incubated for 1.5 hr in a 37°C, 5% CO_2, humidified incubator. The plates were then decanted and washed with 150 μL/well

cation-free PBS. Then 150 μL/well HNGT Buffer (50 mM HEPES pH 7.5, 150 mM NaCl, 10% glycerol, 1%Triton-X,) with

1x HALT Protease/Phosphatase Inhibitor Cocktail (Pierce #78447) was added. Plates were heat sealed and placed on a rotary

plate shaker for 15 min with vigorous shaking, then centrifuged at 3000 rpm for 5 min and placed in a -80°C freezer until the

ELISA was performed. ELISA plates were prepared the day before the assay by coating black high-binding 96-well plates

(Greiner #675077) with 75 μL/well anti-FLAG antibody (Sigma #F3165) at 5 μg/mL in 0.5M carbonate/bicarbonate buffer,

pH 9.6 and incubated overnight at 4°C. The next day the anti-FLAG-coated plates were washed of primary antibody using an

ELX-405 PlateWasher and wash buffer (1x TBS/0.05% Tween-20 buffer; 5 x 100 μL/well). Plates were then blocked with

75 μL/well 5% BSA in wash buffer for 1 hr at RT. Blocking buffer was removed and cell lysate added (50 μL/well) for 1 hr

at RT. Plates were washed 5 x 100 μL/well and 50 μL/well of anti-Phospho-Threonine antibody (Cell Signaling Technology

#9381s) diluted 1:1,500 in wash buffer was added and incubated for 1 hr at RT. Plates were washed as above and then and

then 50 μL/well Donkey anti-Rabbit antibody (Jackson #711-036-152) diluted 1:4,000 in wash buffer was added to the wells

and incubate 1 hr at RT. After washing as above, 50 μL/well 1x SuperSignal ELISA Pico Substrate (Pierce #37069) was

added. Following a 5-min incubation, plates were read on a Perkin-Elmer Envision using 96-well luminescence protocol.

Where not specified above, chemicals were purchased from Sigma. Percent inhibition was calculated based on sample wells

containing either DMSO only (0% inhibition) or a standard compound (100% inhibition). Compound concentration-

responses were fit using a 4-parameter equation to calculate IC_{50} values.

Mouse LPS Model. Male mice (C57/Bl6) were obtained from Charles River Laboratories. Mice (n=6-8 per group) were

administered compound by oral gavage followed by intravenous injection (10,000 U/kg) of LPS (Invivogen, *E. coli*

O111:B4) 30 minutes later. Blood samples for TNF-α analysis were obtained by terminal cardiac bleeding 90 minutes post

LPS administration. Mouse plasma TNF-α concentrations were determined by ultra-sensitive MSD cytokine assay (MSD, K153BHC-1). The data are presented as the mean ± SE and statistical analysis was performed using GraphPad Prism 5. One-way ANOVA with Bonferroni's posttests were used for statistical analysis and $P < 0.05$ were considered statistically significant. All procedures performed on these animals were in accordance with regulations and established guidelines and were reviewed and approved by Pfizer Institutional Animal Care and Use Committee.

Synthetic Materials and Methods. All chemicals, reagents and solvents were purchased from commercial sources and used without further purification. All reactions were performed under an atmosphere of nitrogen unless otherwise noted. Proton (^{1}H NMR) nuclear magnetic spectra were recorded with 400 MHz and 500 MHz Varian spectrometers. Chemical shifts are reported in parts per million relative to the residual solvent signals (i.e. for CDCl$_3$ δH = 7.27 ppm, for DMSO-d_6 δH = 2.50 ppm and for CD$_3$OD δH = 4.78 and 3.31 ppm). The peak shapes are denoted as follows: s, singlet; d, doublet; t, triplet; q, quartet; m, multiplet; br s, broad singlet. Mass spectrometry (MS) was performed via atmospheric pressure chemical ionization (APCI) or electrospray ionization (ESI) sources. Liquid chromatography mass spectrometry (LCMS) was performed on an Agilent 1100 Series (Waters Atlantis C18 column, 4.6 x 50 mm, 5 μm; 95% water/acetonitrile linear gradient to 5% water/acetonitrile over 4 min, hold at 5% water/ 95% acetonitrile to 5.0 min, trifluoroacetic acid modifier (0.05%); flow rate of 2.0 mL/ min) and ultra-pressure liquid chromatography mass spectrometry (UPLC-MS) was performed on a Waters Acquity System (Waters Acquity HSS T3 C18 column, 2.1 x 50 mm, 1.7 μm; 95% water/acetonitrile linear gradient to 5% water/acetonitrile over 1.0 min, hold at 5% water/95% acetonitrile to 1.5 min, formic acid modifier (0.1%) or ammonia modifier (0.1%); flow rate of 1.25 mL/min. Silica gel chromatography was performed using a medium pressure Biotage or ISCO system using columns pre-packaged by various commercial vendors including Biotage and ISCO. Whatman pre-coated silica gel plates (250 μm) were used for analytical TLC. Compound purity was determined by HPLC, with all compounds determined to be ≥95% pure. HPLC purity determination methods are described in the *Supporting Information* section. The syntheses of compounds **1**, **2**, **3** and **7** were previously reported.[13] Compound **37** (catalog #PZ0283) is commercially available via Sigma Aldrich.

6'-Amino-5'-(4-chlorophenyl)-3,3'-bipyridine-6-carboxylic acid, hydrochloride salt (3). A 4 M solution of HCl in EtOAc (0.31 mL, 1.26 mmol) was added to a mixture of **45** (120 mg, 0.31 mmol) in DCM (5 mL). After the reaction mixture had been stirred at RT for 16 h, it was concentrated, and the resulting solids were triturated with DCM (10 mL) to provide the title compound (37 mg, 0.11 mmol, 35%) as a white solid. ^{1}H NMR (400 MHz, DMSO-d_6) δ 9.2 (s, 1H), 8.65 (s, 1H), 8.4–8.3 (d, 1H), 8.35 (s, 1H), 8.2–8.1 (d, 1H), 8.2–7.9 (br s, 3H), 7.65 (br s, 4H); LCMS: [M+1] = 326.1; Purity: HPLC Method C, 97.1%.

4-(6-Amino-5-phenylpyridin-3-yl)benzoic acid, TFA salt (12). To a solution of **54** (40 mg, 0.12 mmol) in DCM (2 mL) was added TFA (0.4 mL), and the reaction mixture was stirred at 30 °C for 1 h. Concentration afforded the title compound (30 mg, 74 μmol, 62%) as a yellow solid. ^{1}H NMR (400 MHz, DMSO-d_6) δ 8.45 (d, J = 2.0 Hz, 1H), 8.22 (d, J = 2.0 Hz, 1H), 7.98–8.05 (m, 2H), 7.91 (d, J = 8.5 Hz, 2H), 7.72 (br s, 2H), 7.48–7.61 (m, 5H); LCMS: [M+1] = 290.9; Purity: HPLC Method A, 98.8%.

2-{4-[6-Amino-5-(4-chlorophenyl)pyridin-3-yl]phenoxy}-2-methylpropanoic acid (37). A suspension of **49** (30.3 g, 73.7 mmol) in EtOH (180 mL) was treated with 4 M NaOH (55.3 mL), and the reaction mixture was heated at reflux for 45 min. Upon reaching reflux temperature the solids dissolved, providing a pale yellow solution. The reaction was cooled to 60 °C and titrated to pH 3.5 with 5 M HCl (approximately 45 mL). A very thick, pale yellow precipitate formed and the mixture was allowed to stir for 4 h at 60 °C. The solids were collected by filtration and dried overnight in a vacuum oven to deliver the hydrate of the title compound (26.34 g, 68.80 mmol, 93%) as a crystalline white solid. ^{1}H NMR (400 MHz, DMSO-d_6) δ 13.07 (br s, 1H), 8.24 (d, J = 2.3 Hz, 1H), 7.45–7.63 (m, 7H), 6.86 (d, J = 8.6 Hz, 2H), 5.75 (s, 2H), 3.32 (br s, 2H water peak), 1.52 (s, 6H); ^{13}C NMR (101 MHz, DMSO-d_6) δ 175.0, 155.4, 154.3, 144.8, 136.9, 135.5, 132.0, 131.1, 130.5, 128.8, 126.5, 125.0, 119.1, 118.9, 78.5, 25.1; LCMS: [M+1] = 383.1; Purity: HPLC Method E, 98.1%. Anal. Calcd for $C_{21}H_{19}ClN_2O_3 \cdot H_2O$; C, 62.92; H, 5.28; Cl, 8.84; N, 6.99. Found C, 62.89; H, 5.26; N, 6.96.

tert-Butyl 6'-amino-5'-(4-chlorophenyl)-3,3'-bipyridine-6-carboxylate (45). To a mixture of 3-(4-chlorophenyl)-5-(4,4,5,5-tetramethyl-1,3,2-dioxaborolan-2-yl)-2-pyridinamine (**43**)[13] (150 mg, 0.45 mmol) in 3:1 dioxane/H_2O (4 mL) were added *tert*-butyl 5-bromopyridine-2-carboxylate (**44**) (117 mg, 0.45 mmol), Na_2CO_3 (96 mg, 0.91 mmol), and Pd(dppf)Cl$_2$ (33 mg, 45 μmol). After the reaction mixture had been stirred at 85 °C for 6 h, it was cooled to RT, and extracted with DCM (40 mL) {in some of the experiments referencing this procedure, extraction was carried out using EtOAc}; the organic layer was washed with brine, dried over Na_2SO_4, filtered, and concentrated. The crude product was purified via silica gel chromatography (gradient: 0% to 80% EtOAc in petroleum ether) to deliver the title compound (140 mg, 0.367 mmol, 81%) as a yellow solid. ^{1}H NMR (400 MHz, DMSO-d_6) δ 9.01 (s, 1H), 8.46 (s, 1H), 8.3–8.2 (d, 1H), 8.0–7.9 (d, 1H), 7.78 (s, 1H), 7.55 (br s, 4H), 6.11 (s, 2H), 1.56 (s, 9H).

Ethyl 2-(4-bromophenoxy)-2-methylpropanoate (46). A mixture of 4-bromophenol (200 g, 1.16 mol) and K_2CO_3 (191 g, 1.39 mol) in ethyl 2-bromo-2-methylpropanoate (400 mL) was heated at 110 °C for 48 h. The reaction mixture was cooled to RT and filtered through diatomaceous earth; the filtrate was concentrated to provide the title compound (280 g, 0.975 mol, 84%) as a colorless oil, which was used for the next step without purification.

Ethyl 2-methyl-2-[4-(4,4,5,5-tetramethyl-1,3,2-dioxaborolan-2-yl)phenoxy]propanoate (**47**). This reaction was carried out in two batches of the same scale. A suspension of **46** (100 g, 348 mmol), B_2Pin_2 (88.5 g, 348 mmol), and KOAc (85.4 g, 871 mmol) in dioxane (1.5 L) was degassed and refilled with N_2 several times. Pd(dppf)Cl_2 (14.2 g, 17.4 mmol) was added, and the mixture was degassed and refilled with N_2 three times. The reaction mixture was heated to 80 °C for 16 h, and then cooled to RT. The two batches were combined at this point, then filtered and concentrated. After the residue had been partitioned between EtOAc (3 L) and water (1.5 L), the aqueous layer was extracted with EtOAc (1 L), and the combined organic layers were washed with water (2 L) and with brine (2 L), dried over Na_2SO_4, filtered, and concentrated. The crude product was subjected to chromatography on silica gel (Gradient: 0% to 10% EtOAc in petroleum ether), and the purified material was triturated with petroleum ether (600 mL) to deliver the title compound (110 g, 329 mmol, 47%) as a white solid. ^{1}H NMR (400 MHz, CDCl$_3$) δ 7.70 (d, J = 8.5 Hz, 2H), 6.81 (d, J = 8.5 Hz, 2H), 4.22 (q, J = 7.0 Hz, 2H), 1.62 (s, 6H), 1.33 (s, 12H), 1.23 (t, J = 7.3 Hz, 3H); LCMS: [M+1] = 335.2.

Ethyl 2-{4-[6-amino-5-(4-chlorophenyl)pyridin-3-yl]phenoxy}-2-methylpropanoate (**49**). A flask containing **48** (15.0 g, 52.9 mmol), **47** (19.4 g, 58.2 mmol), Na_2CO_3 (16.8 g, 159 mmol), and Pd(AmPhos)$_2$Cl$_2$ (375 mg, 0.53 mmol) was purged with N_2. Degassed 5:1 EtOH/H_2O (180 mL) was added and the reaction mixture was heated at 60 °C for 3 h. It was then diluted with EtOH (150 mL), followed by addition of H_2O (360 mL), and the resulting mixture was allowed to stir while cooling to RT. After approximately 1 h of stirring, the precipitate was collected by filtration and the solids dried overnight under vacuum to deliver the title compound (21.42 g, 52.13 mmol, 99%) as a tan solid. ^{1}H NMR (400 MHz, DMSO-d_6) δ 8.24 (d, J = 2.7 Hz, 1H), 7.48–7.57 (m, 7H), 6.83 (d, J = 8.6 Hz, 2H), 5.75 (s, 2H), 4.18 (q, J = 7.0 Hz, 2H), 1.53 (s, 6H), 1.19 (t, J = 7.2 Hz, 3H); LCMS: [M+1] = 411.2

tert-Butyl 4-(6-aminopyridin-3-yl)benzoate (**52**). Dioxane (180 mL) and aq 2 M Na_2CO_3 (86.7 mL, 173 mmol) were added to a mixture of 2-amino-5-bromopyridine (**51**) (10.0 g, 57.8 mmol) and [4-(*tert*-butoxycarbonyl)phenyl]boronic acid (**50**) (14.1 g, 63.6 mmol). After the solution had been degassed with N_2 for 10 min, Pd(dppf)Cl_2 (2.11 g, 2.89 mmol) was added, and the reaction mixture was heated at 80 °C for 2 h, then allowed to cool to RT. Dioxane was removed via concentration, and the aqueous residue was partitioned between water (500 mL) and EtOAc (300 mL). The aqueous layer was extracted with additional EtOAc (2 x 300 mL), and the combined organic layers were dried over Na_2SO_4, filtered, and concentrated to provide a grey solid, which was taken up in water (500 mL), acidified with 1 M HCl (100 mL), and washed with 1:1 EtOAc/heptane (2 x 300 mL). The organic washes were combined and extracted with 0.2 M HCl (250 mL), and all of the acidic aqueous layers were combined, basified with 8 M aq NaOH, and extracted with EtOAc (3 x 250 mL). These organic extracts were combined, dried over Na_2SO_4, and filtered through a pad of silica gel (250 g) in a 2 L fritted funnel, eluting

with additional EtOAc (2 L). Concentration of the filtrate afforded the title compound (13.87 g, 51.3 mmol, 89%) as a tan solid. ^{1}H NMR (400 MHz, CDCl$_3$) δ 8.13 (d, J = 5.5 Hz, 1H), 8.07 (d, J = 8.6 Hz, 2H), 7.63 (d, J = 8.6 Hz, 2H), 6.91 (dd, J = 5.3, 1.4 Hz, 1H), 6.74 (s, 1H), 4.74 (br s, 2H), 1.62 (s, 9H); LCMS: [M+1] = 272.1.

tert-Butyl 4-(6-amino-5-bromopyridin-3-yl)benzoate (53). Freshly recrystallized NBS (8.78 g, 49.3 mmol) was added portion-wise over 15 min to a solution of **52** (13.34 g, 49.35 mmol) in DCM (400 mL). After the reaction mixture had been stirred for 1 h at RT, it was washed with water (2 x 400 mL) and with 10% aq Na$_2$S$_2$O$_3$ (200 mL). The organic layer was then dried over Na$_2$SO$_4$, filtered, concentrated, and purified using silica gel chromatography (Gradient: 0% to 50% ethyl acetate in heptane). The resulting brown solid was triturated with 10% DCM in heptane (200 mL) to afford the title compound (15.74 g, 45.07 mmol, 91%) as a tan solid. ^{1}H NMR (400 MHz, DMSO-d_6) δ 8.11 (s, 1H), 7.98 (d, J = 8.6 Hz, 2H), 7.51 (d, J = 8.6 Hz, 2H), 6.46 (s, 1H), 6.29 (s, 2H), 1.57 (s, 9H); LCMS: [M+1] = 349.0.

tert-Butyl 4-(6-amino-5-phenyl-3-pyridinyl)benzoate (54). Prepared from **53** (100 mg, 0.29 mmol), phenylboronic acid (22.1 mg, 0.286 mmol), K$_2$CO$_3$ (99 mg, 0.72 mmol), and Pd(dppf)Cl$_2$ (21.0 mg, 29 µmol) in 3:1 dioxane/water (8 mL), according to the method utilized for compound **45**, to afford the title compound (45 mg, 0.13 mmol, 45%) as a yellow oil. ^{1}H NMR (400 MHz, CDCl$_3$) δ 8.37 (d, J = 1.0 Hz, 1H), 8.04 (d, J = 8.0 Hz, 2H), 7.65 (d, J = 1.0 Hz, 1H), 7.60 (d, J = 8.0 Hz, 2H), 7.54–7.46 (m, 4H), 7.46–7.39 (m, 1H), 4.78 (br s, 2H), 1.62 (s, 9H).

▪ ASSOCIATED CONTENT

Accession Code

Atomic coordinates MAP4K4 kinase domain bound to compound **27** (PDB code 5J95) have been deposited with the Protein Data Bank.

AUTHOR INFORMATION

Corresponding Author

*E-mail: robert.l.dow@pfizer.com. Phone:1-617-551-3254.

Notes

ACKNOWLEDGMENTS

ABBREVIATIONS

ACE = angiotensin converting enzyme; ATP = adenosine triphosphate ; BCRP = breast cancer resistance protein; CYP3A4 = cytochrome P450 3A4; MW = molecular weight; TPSA = topological polar surface area; HLM=human liver microsomes; LPS = lipopolysaccharide; bpm = beats per minute; MDCK-MDR1 = Madin Darby canine kidney-multi-drug resistant; PDE=phosphodiesterase; PK/PD = pharmacokinetic/pharmacodynamics; TNFα = tumor necrosis factor alpha.

PDB Code

Compound **27**: 5J95. Authors will release the atomic coordinates upon article publication.

Supporting Information

The Supporting Information is available free of charge on the ACS Publications website at DOI:

Additional information for the HPLC purity analysis conditions, molecular formula strings, experimental procedures for compounds **4-11**, **13-36** and **38-42**, kinome profiles of compounds **25** and **26**, off-target profiles for compounds **4** and **37**, ACE/5HT1B functional profiles of compound **37**, ActivX kinome profile of compound **37**, protein production, purification

and X-ray crystal structure data for compound **37** bound to the kinase domain of MAP4K4 are provided. Atomic coordinates

and experimental data have been released for PDB ID code 5J95.

REFERENCES

(1) Yao, Z.; Zhou, G.; Wang, X. S.; Brown, A.; Diener, K.; Gan, H.; Tan, T. H. A novel human STE20-related protein kinase,

HGK, that specifically activates the c-Jun N-terminal kinase signaling pathway. *J. Biol. Chem.* **1999**, *274*: 2118–2225.

(2) Aouadi, M.; Tesz, G. J.; Nicoloro, S. M.; Wang, M.; Chouinard, M.; Soto, E.; Ostroff, G. R.; Czech, M. P. Orally deliv-

ered siRNA targeting macrophage Map4k4 suppresses systemic inflammation. *Nature* **2009**, *458*, 1180-1184.

 (3) Wright, J. H.; Wang, X.; Manning, G.; LaMere, B. J.; Le, P.; Zhu, S.; Khatry, D.; Flanagan, P. M.; Buckley, S. D.; Whyte,

D. B.; Howlett, A. R.; Bischoff, J. R.; Lipson, K. E.; Jallal, B. The STE20 kinse HGK is broadly expressed in human tumor

cells and can modulate cellular transformation, invasion, and adhesion. *Mol. Cell. Biol.* **2003**, *23*, 2068-2082.

(4) Liang, J. J.; Wang, H.; Rashid, A.; Tan, T.-H.; Hwang, R. F.; Hamilton, S. R.; Abbruzzese, J. L.; Evans, D. B.; Wang, H.

Expression of MAP4K4 is associated with worse prognosis in patients with stage II pancreatic ductal adenocarcinoma. *Clin.

Cancer Res.* **2008**, *14*, 7043-7049.

(5) Bouzakri, K.; Zierath, J. R. MAP4K4 gene silencing in human skeletal muscle prevents tumor necrosis factor-α-induced

insulin resistance. *J. Biol. Chem.* **2007**, *282*, 7783-7789.

(6) Vitorino, P.; Yeung, S.; Crow, A.; Bakke, J.; Smyczek, T.; West, K.; McNamara, E.; Eastham-Anderson, J.; Gould, S.;

Harris, S. F.; Ndubaku, C.; Ye, W. MAP4K4 regulates integrin-FERM binding to control endothelial cell motility. *Nature*

2015, *519*, 425-430.

 (7) Collins, C. S.; Hong, J.; Sapinoso, L.; Zhou, T.; Liu, Z.; Michklash, K.; Schultz, P. G.; Hampton, G. M. A small interfer-

ing RNA screen for modulators of tumor cell motility identifies MAP4K4 as a promigratory kinase. *Proc. Natl. Acad. Sci.

USA* **2006**, *103*, 3775-3780.

(8) Yan, W.; Nehrke, K.; Choik J.; Barber, D. L. The Nck-interacting kinase (NIK) phosphorylate the Na+-H+ exchanger

NHE1 and regulates NHE1 activation by platelet-derived growth factor. *J. Biol. Chem.* **2001**, *276*, 31349-31356.

(9) LeClaire, L. L.; Rana, M.; Baumgartner, M.; Barber, D. L. The Nck-interacting kinase NIK increases ARP2/3 complex activity by phosphorylating the Arp2 subunit. *J. Cell Biol.* **2015**, *208*, 161-170.

(10) Baurmgartner, M.; Sillman, A. L.; Backwood, E. M.; Srivastava, J.; Madson, N.; Schilling, J. W.; Wright, J. H.; Barber, D. L. The Nck-interacting kinase phosphorylates ERM proteins for formation of lamellipodium by growth factors. *Proc. Natl. Acad. Sci. USA* **2006**, *103*, 13391-13396

(11) Schwaid, A. G.; Su, C.; Loos, P.; Wu, J.; Nguyen, C.; Stone, K. L.; Kanyo, J.; Geoghegan, K. F.; Bhattacharya, S. K.; Dow, R. L.; Buckbinder, L.; Carpino, P. A. MAP4K4 is a threonine kinase that phosphorylates FARP1. *ACS Chem. Biol.* **2015**, *10*, 2667-2671.

(12) Ndubaku, C. O.; Crawford, T. D.; Chen, H.; Boggs, J. W.; Brobnick, J.; Harris, S. F.; Jesudason, R.; NcNamara, E.; Nonomiya, J.; Sambrone, A.; Schmidt, S.; Smyczek, T.; Vitorino, P.; Wang, L.; Wu, P.; Yeung, S.; Chen, J.; Chen, K.; Ding, C. Z.; Wang, T.; Xu, Z.; Gould, S. E.; Murray, L. J.; Ye, W. Structure-based design of GNE-495, a potent and selective MAP4K4 inhibitor with efficacy in retinal angiogenesis. *ACS Med. Chem. Lett.* **2015**, *6*, 913-918.

(13) Ammirati, M.; Bagley, S. W.; Bhattacharya, S. K.; Buckbinder, L.; Carlo, A. A.; Conrad, R. Cortes, C.; Dow, R. L.; Dowling, M. S.; El-Kattan, A.; Ford, K.; Guimaraes, C. R. W.; Hepworth, D. Jiao, W.; LaPerle, J.; Liu, S.; Londregan, A.; Loria, P. M.; Mathiowetz, A. M.; Munchhof, M.; Orr, S. T. M.; Petersen, D. N.; Price, D. A.; Skoura, A. Smith, A. C.; Wang, J. Discovery of an in vivo tool to establish proof-of-concept for MAP4K4-based antidiabetic treatment. *ACS Med. Chem. Lett.* **2015**, *6*, 1128-1133.

(14) Schröder, P.; Förster, T.; Kleine, S.; Becker, C.; Richters, A.; Ziegler, S.; Rauh, D.; Kumar, K.; Waldmann, H. Neuritogenic militarinone-inspired 4-hydroxypyridones target the stress pathway kinase MAP4K4. *Angew. Chem. Int. Ed.* **2015**, *54*, 12398-12403.

(15) Guimarães, C. R. W.; Rai, B. K.; Munchhof, M. J.; Liu, S.; Wang, J.; Bhattacharya, S. K.; Buckbinder, L. Understanding the impact of the P-loop conformation on kinase selectivity. *J. Chem. Inf. Model.* **2011**, *51*, 1199-1204.

(16) Aouadi, M.; Tesz, G. J.; Nicoloro, S. M.; Wang, M.; Chouinard, M.; Soto, E.; Ostroff, G. R.; Czech, M. P. Orally delivered siRNA targeting macrophage MAP4K4 suppresses systemic inflammation. *Nature*, **2009**, *458*, 1180-1184.

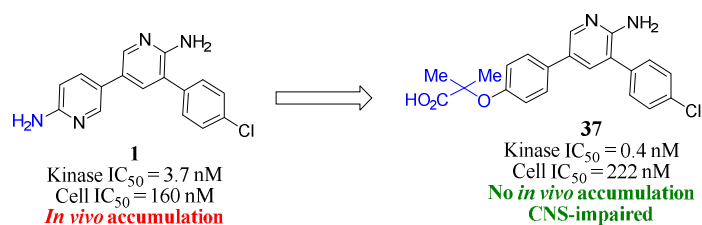(17) Unpublished results on MAP4K4 enzymatic/TDI profiling of ~60 analogs from this chemical series.

(18) Shah, R. R.; Morganroth, J.; Shah, D. R. Cardiovascular safety of tyrosine kinase inhibitors: with a special focus on cardiac repolarisation (QT interval). *Drug Saf.* **2013**, *36*, 295-316.

(19) Percent change in midazolam metabolism by CYP3A4 @ 60, 30, 10, 3 and 1 μM test compound concentrations: **1**: 61%, 54%, 27%, 14%; **5**: 26%, 3%, 1%, -4%, respectively.

(20) Apparent, intrinsic human liver microsomal clearance for **1**, **3**, **4** and **5**: 42, < 8, < 8 and 14 mL/min/kg, respectively.

(21) Di, L.; Whitney-Pickett, C.; Umland, J. P.; Zhang, H.; Zhang, X.; Gebhard, D. F.; Lai, Y.; Fedrico III, J. J.; Davidson, R. F.; Smith, R.; Reyner, E. L.; Lee, C.; Feng, B.; Rotter, C.; Varma, M. V.; Kempshall, S.; Fenner, K.; El-Kattan, A. F.; Liston, T. E.; Troutman, M. D. Development of a new permeability assay using low-efflux MDCKII cells. *J. Pharm. Sci.* **2011**, *100*, 4974-4985.

(22) Given their high ATP-site homology, members of this aminopyridine series also inhibit the other GCK family members (ZC2, TNIK and ZC3, MINK) to a similar degree as MAP4K4.

(23) Orr, S. T.; Rip, S. L.; Ballard, T. E.; Henderson, J. L.; Scott, D. O.; Obach, R. S.; Sun, H.; Kalgutkar, A. S.. Mechanism-based inactivation (MBI) of cytochrome P450 enzymes: structure−activity relationships and discovery strategies to mitigate drug−drug interaction risks *J. Med. Chem.* **2012**; *55*, 4896-4933.

(24) Benbow, J. W.; Aubrecht, J.; Banker, M. J.; Nettleton, D.; Aleo, M. D., Predicting safety toleration of pharmaceutical chemical leads: cytotoxicity correlations to exploratory toxicity studies. *Toxicol. Lett*. **2010**, *197*, 175-182.

(25) Aubrecht, J.; Osowski, J. J.; Persaud, P.; Cheung, J. R.; Ackerman, J.; Lopes, S. H.; Ku, W. W. Bioluminescent Salmonella reverse mutation assay: a screen for detecting mutagenicity with high throughput attributes. *Mutagenesis* **2007**, *22*, 335-342.

(26) Following completion of our work there was a report of an alternative approach to peripherally-restricted MAP4K4 inhibitors: Reference 12.

(27) Kikuchi, R.; de Morais, S. M.; Kalvass, J. C. In vitro P-glycoprotein efflux ratio can predict the in vivo brain penetration regardless of biopharmaceutics drug disposition classification system class. *Drug Metab. Dispos.* **2013**, *41*, 2012-2017.

(28) Zhou, L.; Schmidt, K.; Nelson, F. R.; Zelesky, V.; Troutman, M. D.; Feng, B. The effect of breast cancer resistance protein and P-glycoprotein on the brain penetration of flavopiridol, imatinib mesylate (gleevac), prazosin, and 2-methoxy-3-(4-(2-(5-methyl-2-phenyloxazol-4-yl)ethoxy)phenyl)propanoic acid (PF-0407288) in mice. **2009**, *37*, 946-955.

(29) Miyaura, N.; Suzuki, A. Palladium-catalyzed cross-coupling reactions of organoboron compounds. *Chem. Rev.* **1995**, *95(7)*, 2457-2483.
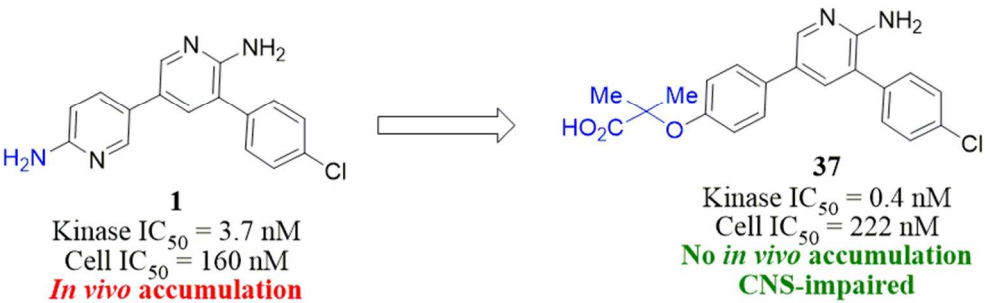
1
2
3
4
5
6
7
8
9
10
11
12
13
14
15
16
17
18
19
20
21
22
23
24
25
26
27
28
29
30
31
32
33
34
35
36
37
38
39
40
41
42
43
44
45
46
47
48
49
50
51
52
53
54
55
56
57
58
59
60

Table of Contents Graphic

1
Kinase IC$_{50}$ = 3.7 nM
Cell IC$_{50}$ = 160 nM
In vivo **accumulation**

37
Kinase IC$_{50}$ = 0.4 nM
Cell IC$_{50}$ = 222 nM
No *in vivo* accumulation
CNS-impaired

1
Kinase IC$_{50}$ = 3.7 nM
Cell IC$_{50}$ = 160 nM
In vivo accumulation

37
Kinase IC$_{50}$ = 0.4 nM
Cell IC$_{50}$ = 222 nM
No *in vivo* accumulation
CNS-impaired

74x23mm (300 x 300 DPI)